

# 1

## *Long Circulating Nanoparticles for Tolerogenesis*

Amy Tekrony<sup>1</sup>; Vincent Wright<sup>2</sup>; Anne Slaney<sup>2</sup>; Usama Al-Atar<sup>2</sup>; Amy Frederick<sup>1</sup>; Teresa Rodriguez<sup>1</sup>; Jillian Buriak<sup>2</sup>; David Cramb<sup>1,4</sup>; Lori West<sup>3</sup>

1. Department of Chemistry, University of Calgary
2. Department of Chemistry, University of Alberta
3. Departments of Pediatrics, Surgery, and Immunology, University of Alberta
4. Corresponding author.

### Outline:

Introduction.....	2
Blood Type Antigens and Immunology .....	2
Nanoparticles for Tolerogenesis .....	6
Methods .....	8
<i>Nanoparticle Design and Synthesis</i> .....	8
<i>Nanoparticle Characterization in Solution</i> .....	10
<i>CAM preparation</i> .....	11
<i>S2.4. Microinjection</i> .....	11
<i>Chicken Embryo Chorioallantoic Membrane (CAM) Model for Nanoparticle Characterization</i> .....	12
<i>FCS Analysis</i> .....	12
<i>S2.5. Zeta-Potential Measurement</i> .....	12
Results and Discussion .....	12
<i>Nanoparticle stability in aqueous solution and blood sera</i> .....	12
<i>Nanoparticles in the CAM</i> .....	14
Conclusion.....	17
Acknowledgements .....	17
References.....	17

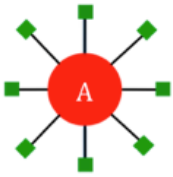
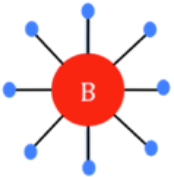
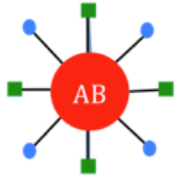
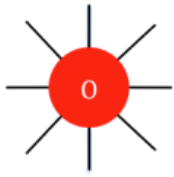
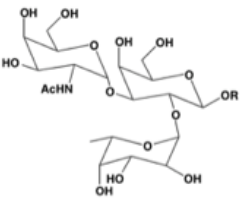
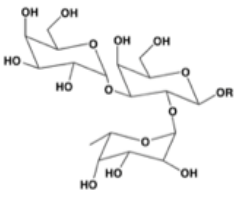
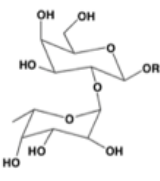
## Introduction

### Blood Type Antigens and Immunology

Blood types are determined by blood type antigens, or sugars, that are expressed on membrane proteins or glycolipids and can be found on red blood cells, epithelial cells, soluble glycans, and other non-erythroid tissue [1, 2]. These sugars are oligosaccharide moieties that are formed on precursor backbones by glycoprotein enzymes in the Golgi apparatus. In humans, there are three blood type antigens: the A, B, and H antigens. The A and B antigens come from the same family, while the H antigen is from a different family of sugars and is a precursor for the other two. Figure 1.1 shows the structures of the A, B, and H antigens, which make up A, B, and O blood types, respectively [3]. The subtle differences of the ABH antigens as seen in Figure 1.1 make up for major differences in antigenicity. These differences can result in an immunological response mediated by natural antibodies, which leads to the rejection of foreign blood and organs in transfusions and transplants [1]. As seen in Table 1.1, only certain blood types are compatible with others [4]. For example, if an A-antigen is already expressed in the recipient, the recipient is able to accept A-type blood without rejection since there will be very few or no anti-A antibodies. However, if the A-antigen is not present, natural anti-A antibodies, present in humans with a healthy immune system, recognize the antigen as foreign. As a result, this recognition and the binding of the anti-A antibody to the A-antigen will induce an immunological response called hyperacute rejection [1, 2, 5]. In people with A-blood type, mostly anti-B antibodies are present in the blood, for B-blood type, mostly anti-A antibodies are present, and for O-blood type, anti-A and anti-B antibodies are present. Although it was previously thought that natural antibodies that react with someone's own antigens were not present in the immune system, there is some evidence that serum contains these natural antibodies (i.e. anti-A antibodies in type A blood type); however, these responses are not pathological when only low levels are present in the blood [2]. As a result of these immune responses to foreign blood type antigens, O-blood type is the universal donor and AB-blood is the universal acceptor (Table 1.1).

**TABLE 1.1**  
Blood type compatibility

<b>Variable</b>	<b>Compatible Blood Groups</b>	<b>Incompatible Blood Groups</b>
<b>Recipient's Blood Type</b>		
<b>O</b>	O	A, B, AB
<b>A</b>	A, O	B, AB
<b>B</b>	B, O	A, AB
<b>AB</b>	AB, B, A, O	N/A
<b>Donor's Blood Type</b>		
<b>O</b>	O, A, B, AB	N/A
<b>A</b>	A, AB	O, B
<b>B</b>	B, AB	O, A
<b>AB</b>	AB	O, A, B

Blood Type				
Antigens Expressed	 A antigen	 B antigen	A and B antigens	 H antigen
Antibodies Produced	 Anti-B Antibody	 Anti-A Antibody	No Antibodies	 Anti-A and Anti-B Antibodies

**FIGURE 1.1**

Structures of the O (H), A, and B blood type antigens for each blood type and resulting antibodies produced in healthy immune system. R = glycoprotein or glycolipid

The antibody responses in the immune system, as described above, play a large role in incompatible blood type transplantation, which results in natural antibody-mediated hyperacute rejection by pre-existing antibodies in the blood. Immunology is a very complex subject, and as a result, organ rejection is also very complex, and factors other than natural antibody-mediated rejection, such as cellular-mediated acute rejection of the human leukocyte antigen (HLA) and chronic rejection [4], also play large roles in graft rejection. However, for the purposes of this chapter, only a general overview of antibody-mediated hyperacute rejection will be given.

In antibody-mediated hyperacute rejection, the binding of an antibody to a foreign antigen can lead to immediate graft destruction within minutes of the antibody recognizing the antigen. Most hyperacute rejection responses occur within 24 hours of transplantation [5]. Graft function is lost as a result of a biochemical cascade that helps the antibodies to clear pathogens, which begins when anti-donor antibodies bind to blood vessels to activate the complement system in the newly transplanted organ. Endothelial cell activation then promotes coagulation by the deposition of fibrin, the formation of microthrombi, and the shedding of thrombomodulin and heparan sulfate proteoglycan, which lead to the infarction of the transplanted organ. Destruction of the vascular endothelium can also lead to oedema and haemorrhage in the tissue. This cascade also causes inflammation, which impairs blood flow to the new organ. The severity of the hyperacute rejection is dependent on the levels of antibodies in the blood stream and the type of antibody expression [2, 5].

Due to a need for donor organs, attempts to cross the ABO barrier have been made, especially in renal transplantation of which failed attempts are not typically fatal [6]. For a successful incompatible transplantation, many immunosuppression techniques must be used such as the administration of

tacrolimus, mycophenolate, and steroids for pretransplant immunosuppression, administration of rituximab for B-cell depletion, and plasmapheresis and immunoadsorption for antibody removal. Even with these measures in place, it is likely that antibodies return due to B-cell memory [6]. Before West *et al.* attempted incompatible infant heart transplants in 1996, intentional incompatible heart transplantation had never occurred due to the obvious fatal consequences of a failed transplant and the susceptibility of heart transplants to hyperacute rejection. Only eight cases worldwide had been previously reported of incompatible heart transplantation, all in adult patients [7], and none were intentional as all of these cases were a result of failure to correctly record either donor or recipient blood type. Six out of the eight patients died as a result of hyperacute rejection to the incompatible transplants [7].

The need for donor organs, especially hearts, is high for infants due to high wait list mortality for this age group. Infants with lethal cardiac disease often die before transplantation due to a shortage of donor hearts. Figure 1.2 shows that most children who die on heart transplant waiting lists are less than 10-15 kg, indicating that infants and toddlers have the highest wait list mortality rates. In addition, infants with type O blood type experience disproportionate compatible donor organs since they can only receive heart transplants of blood type O. Also, many blood type AB donor organs are wasted since they are only compatible with AB blood type recipients [8].

In 1996, West *et al.* successfully attempted to cross the ABO barrier in infants, due to the underdeveloped nature of their immune systems [4], as infants do not produce isohemagglutinins, and anti-A and anti-B antibodies exist in very low levels up until 12-14 months of age. In addition, the complement system of infants is not fully developed at a young age [9]. As a result, it is easier to manipulate the immune systems of infants and ensure that they do not execute a normal immune response, or hyperacute rejection, to foreign antigens in the blood. Therefore, it was hypothesized that the ABO blood barrier could be breached, if done carefully, with the knowledge that the transplanted organ is of incompatible blood type [4]. Between the years of 1996 to 2000, West *et al.* commenced the first study of its kind in which incompatibles hearts were transplanted into young infants whose situations would be fatal otherwise.

Knowing that the transplanted organs were of incompatible blood type had a distinct advantage over the 8 adult cases, which were mostly fatal, since preparations could be made in order to suppress the immune system, keep track of antibody levels, and transfuse the appropriate (donor) blood type into the recipient [4]. Patients from the transplantation waiting list were tested for the presence of anti-A and anti-B antibodies using standard agglutination tests. Those with no or very low levels of antibodies were considered for the study. In addition, antibody levels were tested for each recipient; a. periodically over the waiting period, b. when a potential donor was identified, c. immediately before the surgery, d. continuously during the surgery, e. and every six hours for four days after the surgery in order to ensure that the graft would not be rejected via antibody-mediated hyperacute rejection. In order to prepare for the bypass surgery, the bypass circuit was primed with the blood type of the donor organ or with AB-type blood so that no anti-donor antibodies would be present at the time of the surgery, and the recipient's blood was removed via the bypass circuit and replaced with the donor blood type for the duration of the surgery.

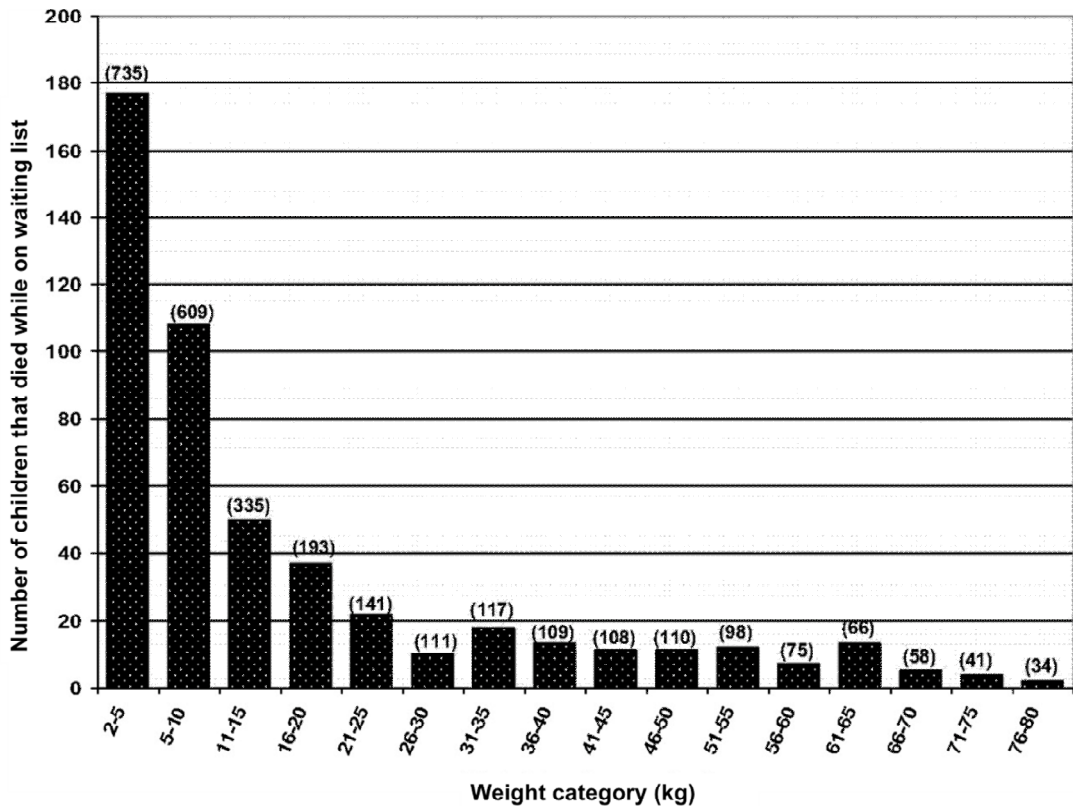


**FIGURE 1.2**

Number of children who died while on the waiting list between 1999 and 2006 according to weight at listing. The numbers above each bar denote the total number of children who were listed for heart transplant within each weight category reproduced with permission from [8]

The patients were also succumbed to intensive immunosuppressive treatment during and post-operation, which was reduced over time. In addition to testing for antibody levels post-operative to monitor any possible antibody-mediated rejection, patients underwent biopsies to rule out chronic rejection within six months after the transplant and then annually after that. All in all, for this study, ten patients between the ages of four hours to fourteen months old underwent ABO-incompatible transplantation and were compared to ten patients between the ages of two months to twelve months who underwent ABO-compatible transplantation from 1996 to 2000 [4].

Initial findings indicated that none of the patients experienced hyperacute rejection. Higher incidences of cellular rejection actually occurred in the ABO-compatible group than in the ABO-incompatible group, possibly due to less intensive immunosuppressive therapy or the slightly higher mean age of the ABO-compatible group. There was also no antibody-mediated chronic rejection observed in either group [4]. Since the time when the initial study was published in 2001, additional results from a total of 35 patients that have undergone ABO-incompatible transplantation and 45 patients that have undergone ABO-compatible transplantations have been analyzed and published. It was found that the freedom from death and transplantation rates were very similar for the two groups at 77% and 74%, respectively for the ABO-incompatible transplantation group and 84% and 74% for the ABO-compatible group [10]. These percentages were found to have no statistical difference. Out of the larger group of

ABO-incompatible transplants, only 2 patients had antibody-mediated rejection and both episodes were handled easily via immunosuppressive techniques. Cellular rejection episodes were similar between the two groups. Of the patients that died, none of them did so as a result of ABO-incompatibility [10]. From these results, it is apparent that this study was a success and that infants' immune systems are at an immaturity level that allows for the ABO barrier to be crossed in transplantation.

Not only was the ABO-barrier crossed successfully as a result of incompatible transplantation, but an induced tolerance to donor antigens was also observed in the infant recipients. It has been known for many years that induction of antigen tolerance is possible in animals. In 1945, Owen defined the inherent susceptibility that animals have to immune tolerance [11]. In 1949, Burnet and Fenner linked this tolerance to developmental events, using twin fetal cows [12], and in 1953, Medawar showed that this tolerance could be induced intentionally in mice [13]. Up until now, these findings were not considered to be clinically relevant to humans since human neonates were considered to have an increased maturity of their immune systems at birth, and therefore, were thought to be beyond susceptibility to tolerance induction. However, as previously stated, human infants' immune systems do show signs of immaturity, such as low or no levels of isohemagglutinins within the first month after birth. This study showing successful incompatible heart transplants was the first to refute what was previously thought and provide evidence for neonatally acquired donor-specific immune tolerance in humans [14]. Fan *et al.* also provide evidence that suggests persistent exposure to donor antigens is required for tolerogenesis (induction of immune tolerance), which is also dependent on the degree of antigen expression [10].

## Nanoparticles for Tolerogenesis

Since evidence shows that the occurrence of tolerogenesis is dependent on degree of antigen exposure, it may be possible to induce tolerance via methods other than graft exposure or transplantation, thereby possibly reducing mortality rates on transplantation wait lists. If an infant must wait for an organ past the time of susceptibility to induced tolerance, it may be beneficial to induce tolerance early in the child's life to allow for tolerance to both A and B antigens, or essentially make that infant's blood type a "universal acceptor". This would increase the likelihood of transplantation at a later point in time when a donor organ may be available, thereby decreasing the likelihood of a fatal outcome.

In order to achieve this goal, it is essential to determine novel methods of tolerance induction. Since lone antigens in the blood stream would likely be cleared quickly by the renal system, our study investigates the possibility of injecting nanoparticle-antigen conjugates into the blood stream to induce tolerance. Ideal particles will be easily detected in order to track them in the blood stream for characterization purposes and circulate for a prolonged period of time in vasculature to ensure maximum exposure to blood stream antigens [3]. Therefore, since polyethylene glycol (PEG) coatings have been shown to increase nanoparticle (NP) circulation time in the blood stream, the majority of the NPs in this study were silica functionalized on their surfaces with PEG [15]. Silica has demonstrated biocompatibility [16] and silica NPs are easily tuned for size [17]. Also, most NPs synthesized contain fluorescent dyes for detection in order to monitor and assess their localization and circulation behaviour.

Previous NP circulation studies have been performed either in adult animals [18] or in tumor models [19]. Neither of these are the most relevant to model neonatal blood circulation. Neonates will have varying degrees of natural angiogenesis, which is modeled poorly by tumor models and not at all by

adult animals. Desirable is a simple angiogenic model into which NPs can be injected and tracked for circulation time, aggregation behavior and general NP stability. The chorioallantoic membrane (CAM, Figure 1.3) of the chicken embryo is an excellent model for angiogenesis. Within the CAM the blood pressure is normal and the vessels are not tortuous unlike tumor models and most of the blood vessels in the zebrafish embryo. The CAM serves as the respiratory system for the chicken embryo up until day 19 of the 21 day gestation period, handles any waste products from the embryo, and supplies the embryo with nutrients from the yolk [20]. The CAM has been used as a model to study angiogenesis of explanted tumours and anti-angiogenic drugs [21-27], tumour vascular targeting [28], metastasis [29, 30], ion transport [31], allergens [32], transplantation [33], contraceptives [34, 35], effects of hyperglycemia [36], and photodynamic therapy [37]. NPs can easily be injected directly into blood vessels of the CAM through a window cut into the eggshell (Figure 1.3). The concentration of the injected particles is then monitored over time using fluorescence correlation spectroscopy (FCS), and it has been shown that the relative concentration of certain particles decreases exponentially within the first few minutes of injection [38]. This exponential decrease of NP concentration is due to loss of the NPs from the blood stream through the angiogenic fenestrations ( $\sim 500\text{nm}$  in size) [39]. The presence of angiogenesis in these developing vessels allows us to find ideal NPs that will circulate for a prolonged period of time, despite the “leaky” nature of the developing vessels. As mentioned above, NP concentration in the CAM can be monitored through the window in the shell using FCS.

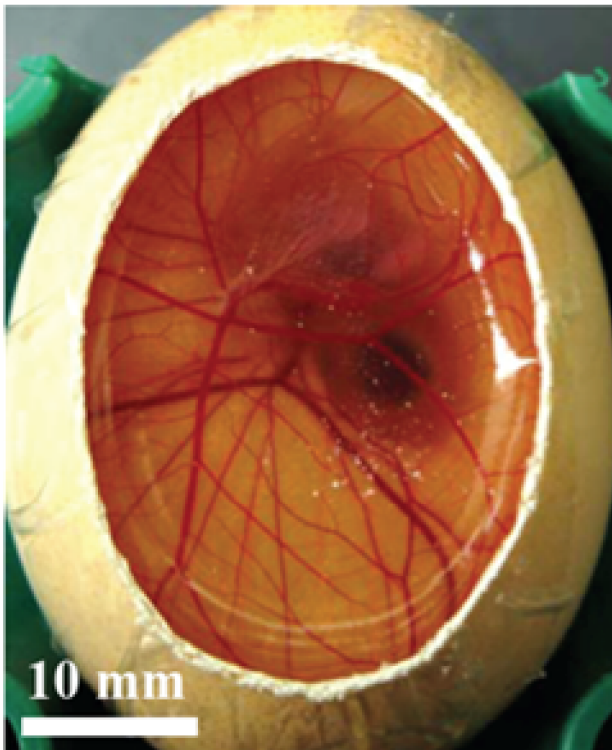


**FIGURE 1.3**

Day 9 embryo with window for experimentation. NP concentration can be determined through the window cut into the shell using FCS on the exposed CAM blood vessels above the embryo

Two-photon excitation (TPE)-FCS is a non-invasive fluorescence technique commonly used to analyze fluorescent particles in living organisms, primarily for advantages such as: low phototoxicity, long-term analysis and ability to distinguish aggregation [38]. TPE-FCS involves analysis of fluorescent intensity fluctuations resulting from two-photon excitation of fluorescent molecules to obtain data about diffusion, concentration, and size of the fluorophores. TPE-FCS has been used to gain valuable information in many applications such as the examination of angiogenic blood vessel formation in zebrafish; the study of active transport, localization of proteins, and diffusion of receptor clusters in cells; monitoring drug delivery using photocages; and the study of DNA replication [40].

In this study, TPE-FCS is used as the primary technique to provide minimally invasive monitoring of NP behaviour in the CAM of the chicken embryo. By tracking the change in concentrations and aggregation tendencies as functions of size and surface chemistries, we may determine which NPs are most easily detected, aggregate the least, and circulate in the blood stream the longest. These data will allow us to predict the NP properties most suitable to provide maximum blood exposure to the synthesized antigens used to induce immunological tolerance in infants.

## Methods

### *Nanoparticle Design and Synthesis*

Various NPs were synthesized with multiple dyes, ratios of dye to silica, surface functionalization, and dye-incorporation methods (See Table 1.2 for the naming system for nanoparticles, according to their synthesis). NPs with dye incorporation were synthesized according to the Stöber process [41], which involves the hydrolysis of alkyl silicates, followed by the condensation of silica acid in alcohol using ammonia as a catalyst. This synthesis resulted in uniform particles of which sizes can be controlled from approximately 0.05  $\mu\text{m}$  to 2  $\mu\text{m}$  in diameter [41]. In order to synthesize the core-shell particles, a modified version of the Stöber process was used, as described by Larson *et al.* [42], in which the dye-rich compact core is synthesized prior to the silica shell. The NPs were functionalized by directly adding polyethylene glycol (PEG) or APTMS to the synthesis flask, which formed covalent bonds from the polymers to the NPs as the base-catalyzed silanization occurs [3]. Once synthesized, particles were resuspended in water and stored in scintillation vials covered with aluminum foil to reduce exposure to light.

### Degree of stability of the dye (relative strength of adhesion of the dye to nanoparticle vs potential dissipation of free dye?)

**TABLE 1.2**

Symbols used for naming nanoparticles

Material		Functionalization		Dye Incorporation		Dye	
Symbol	Meaning	Symbol	Meaning	Symbol	Meaning	Symbol	Meaning
Si	Silica	PEG	Polyethylene glycol	R	Random	R6G	rhodamine 6G
Fe	Iron oxide	NR <sub>3</sub>	Amine	C	Core-shell	TRITC	tetramethyl isothiocyanate
		SPEG	Short PEG	NP	Lg NPs from sm NPs	FITC	fluorescein isothiocyanate
		LPEG	Long PEG			AFX	Alexa Fluor®
		NF	No Funct.			Pyr	Pyrene-maleimide

### Two-Photon Excitation Fluorescence Correlation Spectroscopy

TPE-FCS measures the fluctuations of fluorescence in an optically-defined interrogation volume over time. A temporal autocorrelation analysis is performed on the fluorescence data (see Figure 1.4) to generate the autocorrelation decay,  $G(\tau)$ .

$$G(\tau) = \frac{\langle \delta F(t) * \delta F(t + \tau) \rangle}{\langle F \rangle^2} \quad \text{Equation (1)}$$

Where  $\delta F(t)$  is the difference between the instantaneous fluorescence at time,  $t$ , and the average fluorescence intensity,  $\langle F \rangle$ . As the lag time,  $\tau$ , increases,  $G(\tau)$  decreases, and an autocorrelation decay (ACD) curve results. Equation (2) can be used to model the ACD, when the system is dominated by Brownian diffusion determine the diffusion coefficient, size, and concentration of the NPs [43].

$$G(\tau) = \frac{\left[ 1 + \frac{\left( \frac{\tau}{1000} \right) 8D}{r^2} \right]^{-1} \left[ 1 + \frac{\left( \frac{\tau}{1000} \right) 8D}{Z_0^2} \right]^{-1/2}}{\langle c \rangle \left( \frac{\pi}{2} \right)^{3/2} r^2 Z_0} \quad \text{Equation (2)}$$

Where  $r$  is the radius of the ovoid of the two photon excitation volume (perpendicular to the direction of laser propagation),  $Z_0$  is the depth of the ovoid of two photon excitation (in the direction of laser propagation),  $c$  is the local concentration,  $D$  is the diffusion coefficient, and  $\tau$  is the lag time. It is also

important to note from Equation 2 that  $G(0)$  is equal to  $1/N$  (where  $N$  equals the average number of freely diffusing fluorescent particles in the TPE volume). Thus,  $N$  is the equivalent of concentration. Changes in  $N$  over time may indicate the NPs are being taken up into the angiogenic tissue, aggregating or dissolving.

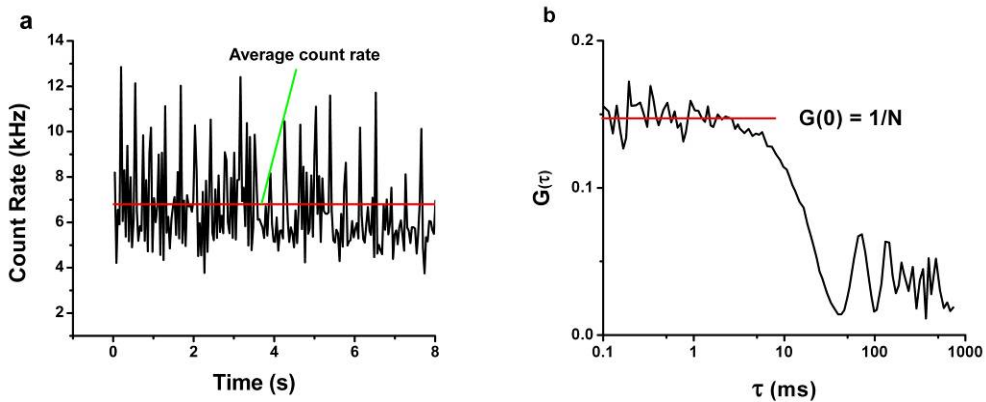


**FIGURE 1.4**

a) Count rate fluorescence trajectory, where the red line is equal to the average count rate and b) Autocorrelation decay curve, where the red line depicts  $G(0)$ , which is equal to  $1/N$ . Both graphs are examples of typical plots that result from FCS analysis of nanoparticle injection into the CAM

To help determine the origin of NP concentration changes we will use the average particle brightness,  $\eta$ . If  $N$  decreases and  $\eta$  increases, this suggests aggregation is taking place. If  $N$  decreases and  $\eta$  remains constant, this suggests uptake or dissolution. And finally if  $N$  remains constant and  $\eta$  decreases this suggests that the fluorescent dye in the NPs is unstable, which could indicate that the NP surfaces are changing. It is simple to calculate the particle brightness (kHz/NP):

$$\eta = 1/N * \langle F \rangle \quad \text{Equation (3)}$$

### **Nanoparticle Characterization in Solution**

In order to assess the suitability of the NPs for injection into the CAM, initial characterization of the NP solutions was first performed in various solutions. If the NPs were unstable in simple solution, they were deemed inappropriate for study in the CAM environment. Particles were diluted to the 10-100 nM concentration range ( $10 < N < 100$ ). This would be the appropriate range for the CAM studies and likely the desirable range for tolerogenesis. Particles that were monodisperse, bright, and gave consistent autocorrelation decay curves in water, were further analyzed in various buffer and sera solutions.

The monodisperse, bright NPs mentioned above were analyzed for their behaviour in phosphate buffered saline (PBS), chicken blood serum (CBS), and porcine blood serum (PorBS) over time to observe possible effects on salts and proteins on the NPs from the buffer and sera, respectively aggregation. FCS measurements were taken at short intervals for the first 30 minutes post dilution and at longer intervals after that over the time span of an hour. Autocorrelation decay curves and count rate trajectories were analyzed for signs of aggregation and changing concentration. Time for complete loss of fluorescence?

### ***CAM preparation***

Fertilized eggs were obtained from the Ijtsma Poultry Farm north of Calgary (RR 284 and highway 72, Mailing address: RR2, Site 11, Box 6, Airdrie, AB, T4B 2A4). Eggs were stored for up to two weeks in a refrigerator at 4°C, at which time they lose viability. Nine days before experimentation, eggs were removed from the refrigerator and allowed to sit at room temperature for a few hours, after which, the eggs were cleaned using a 70% ethanol solution. The eggs were then placed horizontally on egg racks, and the date of experimentation was written on the top center of the egg to allow for a reference point later in the incubation period. The eggs were then incubated at 37 degrees Celsius and approximately 60% humidity. On day four and a half of the incubation period, the eggs were windowed to provide visual observation of the embryo development. In order to do this, eggs were first candled to verify development of the CAM and embryo. If this was not the case, eggs were disposed of. All viable eggs were windowed. The first step of this process involved removing 3 mL of albumen using a BD syringe and 21-gauge needle in order to provide an air sac within the egg, which allowed it to be opened without damaging the embryo. Next, the egg was rotated 180 degrees to allow for the CAM to develop over top of the chicken embryo, and cellulose tape was placed on the new top of the egg. Dissecting scissors were then used to cut a small hole into the tape-covered portion of the egg, creating a window to allow visual observation of the development of the chicken embryo and CAM. Cellulose tape was then used to cover the window in the egg, and the eggs were placed back into the incubator. Over the course of the subsequent incubation period, embryos were monitored. On day nine of incubation, the eggs were removed once again for experimentation. The windows in the eggs were expanded to allow for injection of nanoparticles and monitoring of the injectate via FCS. The top portions of the eggs were further covered with cellulose tape to prevent crumbling of the shell into the amniotic fluid and CAM. Dissecting scissors were then used to cut the shell away to the line of the fluid within the egg, thus providing maximum exposure to the CAM for experimentation.

### ***S2.4. Microinjection***

Injections were performed using a manual microinjector from Sutter Instruments Co. Needles were formed using P-30 Puller (Sutter Instruments Co.), beveled using a K.T. Brown Type Micro-Pipette Beveller, Model BV-10 (Sutter Instruments Co.), and held in place and directed by an x, y, z-manipulator (Sutter Instruments Co., MM-33).

Undiluted nanoparticles (~10 nM) were drawn up into a 3 mL BD syringe, which was then attached to the top of the microinjector. The tubing that leads to the manipulator was primed, and a beveled needle was secured into place at the end of the tubing. The needle was also primed and flow through the tip was verified. The valve leading from the BD syringe port to the micro syringe was opened and nanoparticles were drawn into the micro syringe.

Once the microinjector was set up, an egg was placed in an egg holder on the egg stage of the microscope (In-house design, University of Calgary, [44]) and viewed through the 5X objective with a 1 cm working distance. The needle, adjusted to inject parallel to blood flow. Approximately 100  $\mu$ L of nanoparticles were then injected into CAM blood vessels of approximately 100–200  $\mu$ m in diameter. After successful injections, the objective turret position was changed to the 20X lens and the laser was focused in the center of the blood vessel. The focused laser beam was always several hundred microns downstream from the injection site.

### ***Chicken Embryo Chorioallantoic Membrane (CAM) Model for Nanoparticle Characterization***

The types of NPs that did not aggregate in solution (aggregation analysis described by Clancy *et al.*) [38] and were bright enough to be easily detected were injected into blood vessels of the CAM. The NPs were injected through a window of a chicken embryo egg into the blood vessels of the CAM, which are contiguous with the vessel system in the embryo, and FCS was used to track concentration changes of the NPs within the blood vessels. More precisely, 100  $\mu\text{L}$  of undiluted NP solution was injected into a vessel of approximately 100 to 200  $\mu\text{m}$  in diameter. The injectate was allowed to circulate and distribute throughout the blood stream (30 s,[38]), after which FCS measurements were taken continuously from approximately 3 min post injection to approximately 50 min post injection, with the TPE laser beam focused into the center of the lumen.

#### ***FCS Analysis***

For all experiments, count rate trajectories and autocorrelation decay curves were plotted and analyzed using OriginPro 7.

#### ***S2.5. Zeta-Potential Measurement***

Nanoparticles were diluted to approximately  $10^{-10}$  M concentration from original solutions, and a small amount was drawn into a 3 mL BD syringe. Nanoparticles were then injected into disposable polystyrene cuvettes and inserted into the cell holder in the Nano ZS DLS instrument (Malvern Instruments Ltd). Zeta-potentials were obtained in water using averaged data from approximately 80 accumulated data points and pre-assigned settings for silica nanoparticles with the refractive index set to 1.5, the refractive index of silica.

## **Results and Discussion**

### ***Nanoparticle stability in aqueous solution and blood sera***

A series of approximately 50 types of NPs that were synthesized with various combinations of sizes, dyes, surface functionalizations, polymer materials, and synthesis methods, were analyzed for stability in aqueous solution and blood sera. For the purpose of this chapter, the key findings for aqueous solution are presented in Table 1.3, which gives average particle brightness and the percentage of particles that aggregated and were used in eggs based on synthetic particle variables. To sleuth out trends in the characteristics of the NPs, all data for specific characteristics were pooled and then the averages or % displaying the behaviour were calculated. For example, 46 NPs were surface-functionalized with PEG. Their cumulative average  $\square\square$  was 3.5 kHz per particle and 13/46 displayed aggregation in water and 11/46 we ultimately deemed suitable for further study in the CAM. Thus, the results displayed in Table 1.3 were used to help determine which NPs were stable and bright enough for use in the CAM *in vitro* studies.

**TABLE 1.3**

Summary of nanoparticle characterization results in water

\* tetramethyl isothiocyanate, § fluorescein isothiocyanate

Variable		Average particle brightness (kHz/particle)	Percent of particles that aggregated in water	Percent injected into eggs (%)
NP Material	Iron oxide core	0	N/A	0
	Silica	3.2	36	23
Functionalization	PEG	3.5	28	23
	Amine	0.3	80	20
	None	1.3	100	0
Dye-incorporation Method	Core-shell	4.0	41	32
	Random	1.5	0	0
	Large particles made from small ones	0	75	0
Dye	Rhodamine 6G	4.4	32	29
	TRITC* & FITC <sup>§</sup>	1.1	33	16
	Alexa fluor	0.8	50	0
	Pyramine	0.2	50	0
Size	0-75nm	3.7	60	0
	75-200nm	3.9	30	37
	>200nm	0.8	25	8

Out of the fifty particle solutions investigated in this water, twelve types of NPs were mixed with buffer and blood sera to further investigate stability with respect to aggregation in the presence of ions and proteins. Table 1.4 displays the results of these studies.

There was increased particle instability and aggregation in blood serum in comparison to buffer. This was also observed in a study by Eberbeck *et al.*, where they studied magnetic particles in different solutions. It was found that particles had a higher tendency to aggregate in different biological media [45]. However, the results from mixing the silica NPs in different solutions were very promising as a large number of the NPs synthesized showed high stability in PBS and two different blood sera, which was beneficial for the desired purpose of injecting them into the CAM blood vessels.

**TABLE 1.4**

Observed time of nanoparticle aggregation in various solvents over the typical 45 to 60 minutes of data collection, determined from CRT and ACD analysis

Nanoparticle	Approximate time in solution until aggregation is observed (min)		
	PBS	CBS	PorBS
Si_PEG_C_TRITC_89nm	>60	>16	Insufficient data
Si_PEG_C_R6G_105nm	>60	>60	24
Si_PEG_C_R6G_120nm	>60	>60	<6
Si_PEG_C_R6G_125nm	35	45	2
Si_PEG_C_R6G_142nm	>45	45	19
Si_PEG_C_R6G_148nm	>60	23	40
Si_PEG_C_R6G_150nm_2	10	9	<8
Si_PEG_C_R6G_177nm	>60	60	23
Si_PEG_R_TRITC_179nm	>60	15	8
Si_PEG_C_R6G_191nm	>45	45	40
Si_PEG_C_TRITC_250nm	Insufficient data	7	6
Si_PEG_R_R6G_350nm_2	20	11	<16

Overall, only seven out of the total of 50 NPs were deemed appropriate to be injected into the CAM model, which reflects the importance of the specific combination of variables on resulting particle properties. Interestingly, all of the particles that were determined to be suitable for injection were core-shell silica NPs; the core-shell particles tended to be brighter, thus more easily detected for the purposes of this study. All of the NPs injected into the eggs were functionalized with PEG. Five were synthesized utilizing R6G as the dye, while the other two contained TRITC. Also, all NPs stable enough to be injected into the CAM had diameters in between 89 to 250 nm.

### ***Nanoparticles in the CAM***

Based on the above-mentioned results, seven different NPs were studied in the CAM blood vessels. Out of those seven particle solutions, five were found to be stable in the CAM vasculature, with little signs of aggregation over the time periods analyzed (typically around one hour to ensure preservation of the embryo viability).

Figure 1.5a displays a typical plot of the number of silica NPs in the TPE volume,  $N$ , as a function of time for all of the particles injected into the CAM. As demonstrated in Figure 1.5a, there is no indication of any systematic change in particle numbers over the time period (33 min) for this particular NP. The large scatter in the data (average  $\pm$  50%) (Figure 1.5a) results from a number of factors: inhomogeneities in the concentration in time due to pulsatile flow, movement of the embryo and some degree of aggregation. Recall that the angiogenic blood vessels of the CAM possess fenestrations that are 500 nm in diameter or smaller [44]. Therefore, NPs smaller than this size could leave the blood stream through these nanofenestrations. Figure 1.5b, by comparison shows dioleoylphosphatidyl-

serine (DOPS) liposomes ( $\zeta = -59$  mV and 100 nm diameter) injected into the CAM. In the case of DOPS, there is clearly a slow decrease in  $N$  over time, which we have previously shown is due to uptake into the angiogenic blood vessel walls [39].

Data on a Hemolysis assay?

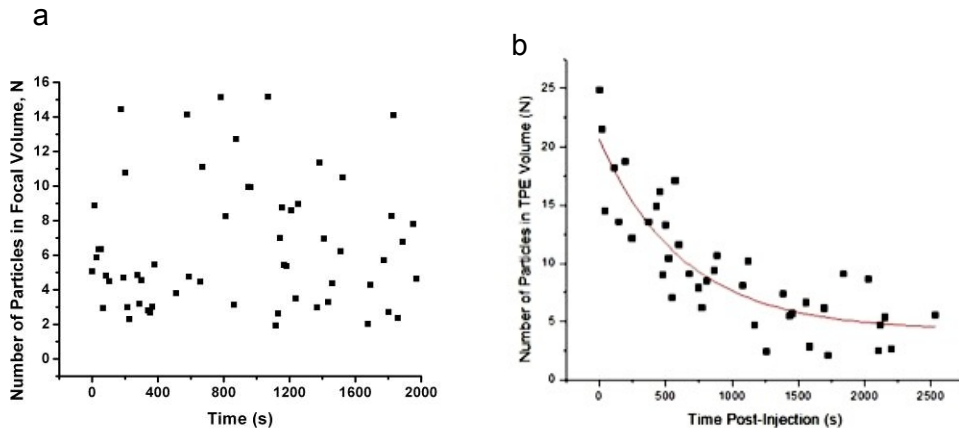


**FIGURE 1.5**

Number of particles in focal volume versus time post injection into eggs for a) 89 nm core-shell TRITC silica particles with PEG functionalization. b) 102 nm diameter DOPS liposomes loaded with lissamine. Red curve represents monoexponential decay fit with rate constant,  $k = 0.002 \text{ s}^{-1}$

The lack of verifiable uptake for these NPs in the CAM is quite significant, since this is not the case with most particles of similar sizes studied by Yaehne *et al.* [46]. In this previous study, we found that many different NPs were taken up into the angiogenic tissues. These particles included PEGylated quantum dots, polystyrene fluospheres and liposomes [39]. It is emerging that size, functionalization, and surface potential all play a large role in the observed uptake rates. We have shown previously that uptake rates have been found to be dependent on size for particles with zeta potentials in the range  $0 < \zeta < -40$  mV [39]. The silica NPs in the current study are of similar sizes to these NPs, but do not deposit in the vessel walls. We therefore propose that there is a negative charge cut-off, which plays a significant role in keeping the NPs in the blood stream. This cut-off appears to be around -50 to -60 mV as discussed in [39], and shown in Table 1.5 as particles with high negative charges are not taken up readily. These findings are likely a result of the large negative zeta potentials of the NPs causing repulsion with the negatively charged endothelial cells making up the blood vessel walls. Furthermore, large surface charge could help to stabilize NPs as the NP-NP repulsion would reduce aggregation. Since many of the non-silica particles in our previous study that displayed uptake are coated with PEG and are of similar diameters [39], this charge effect is likely a significant reason for the differences in circulation behaviour. This result is also supported by the contrast in the results for the circulation behavior of liposomes. The zwitterionic dioleoylphosphatidyl-choline (DOPC,  $\zeta = -40$  mV, 100 nm diameter) left the blood stream with a rate constant of  $k_{\text{loss}} = 0.003 \text{ s}^{-1}$  [39], whereas the DOPS liposomes ( $\zeta = -59$  mV, 100 nm diameter) lasted 50% longer in circulation,  $k_{\text{loss}} = 0.002 \text{ s}^{-1}$  (Figure 1.5). The charge-induced, long circulation time is a very beneficial characteristic for tolerogen carriers, as it would permit maximum exposure of B-cells to NP-conjugated antigens.

Lack of uptake does not necessarily mean complete stability of the silica NPs during circulation. Some were observed to display a degree of aggregation after prolonged exposure to the CAM blood stream. Table 5 gives the length of time during circulation before aggregation of the NPs is observable. This represents the onset of 20-20% aggregation of the NPs. From Table 1.5, it is evident that PEG-coated NPs in the size range 120-150 nm diameter were optimal for better stability against aggregation. Other PEG-functionalized particles, similar to the silica NPs used in this study, have shown similarly long circulation times in other animal models. For example, Maldiney et al. studied the effects of diameter and surface coating on biodistribution within healthy mice [47]. As part of the study, the biodistribution of intravenously administered silicate-based NPs coated with PEG (chain length approximately 10 times longer than the ones used in this study) was compared to that of particles with exposed hydroxyl groups. It was found that PEG-functionalized particles circulated in mice for a longer period of time than the similar hydroxyl-functionalized particles [47]. This was indicated by the rapid uptake of the hydroxyl-coated particles into the liver and a high distribution of the PEG functionalized particle throughout the rest of the organism [47].

**TABLE 1.5**

Zeta potentials and observed time of nanoparticle aggregation in the CAM over the typical 45 to 60 minutes of data collection, determined from CRT and ACD analysis

Nanoparticle	Approximate time (post injection) until aggregation is observed (min)	□ (SD, mV)
Si_PEG_C_TRITC_89nm	25	-64 (20)
Si_PEG_C_R6G_105nm	45	Insufficient data
Si_PEG_C_R6G_120nm	>45	-60 (10)
Si_PEG_C_R6G_125nm	>45	-47 (15)
Si_PEG_C_R6G_150nm_2	>45	Insufficient data
Si_PEG_C_R6G_177nm	45	-68 (9)
Si_PEG_C_TRITC_250nm	30	-48 (5)
DOPS liposomes	>45	-59 (12)

Indication of fluorescent life time? (time taken before complete quench of fluorescence?)

Maldiney also found a strong dependence on size with longer circulation times for particles with 120 nm hydrodynamic diameter compared with larger particles (190-230 nm) [47]. Interestingly, their study found that negatively charged, bare silica particles were rapidly deposited in the liver and spleen. We saw little evidence of this for the negative particles in the current study, however our particles did have a degree of PEG coating and the CAM blood volume is very large compared with the organ blood volume.

PEG has been validated in many previous studies as a coating that increases blood stream circulation time of NPs [48-51]. Our previously reported work has demonstrated that amino-terminated PEG coated quantum dots disappear too quickly from the CAM blood stream to measure the uptake rates (10). Intuitively, the amino functionalization would cause particles to be less negative and therefore be attracted to the negative endothelial cells of the CAM blood vessels. It therefore emerges that a combination of PEGylation and large, negative charge promote longer circulation time in angiogenic blood vessels.

## Conclusion

PEGylated silica nanoparticles were studied in the CAM model as a significant step towards developing long-circulating, stable tolerogen carriers. Such NPs would allow for an increased exposure of the blood stream to the antigens they will carry. It was found that PEG-functionalized particles between 90 to 200 nm in diameter with large negative charges produced the desired effects and circulated for long periods of time in CAM blood vessels. PEGylated silica NPs carry a large negative charge likely because of incomplete coverage of the silica surface by PEG. These findings suggest that silica NPs with the above-mentioned qualities would be suitable for tolerogenesis. As a result, these silica NPs will be conjugated to antigens to determine if the resulting exposure will be persistent enough to induce immunological tolerance to foreign blood type antigens.

## Acknowledgements

The authors would like to thank the Natural Sciences and Engineering Council of Canada and the Canadian Institutes of Health Research for their financial support.

## References

1. Cartron JP, Colin Y. Structural and functional diversity of blood group antigens. *Transfus Clin Biol.* 2001;8(3):163-99.
2. Milland J, Sandrin MS. ABO blood group and related antigens, natural antibodies and transplantation. *Tissue Antigens.* 2006;68(6):459-66.
3. West LJ. Research Proposal: Nanomedicine in Organ Transplantation: Polysaccharide Structures as Immunologic Tolerogens for Infant Heart Transplantation. Edmonton, AB: University of Alberta, 2008.
4. West LJ, Pollock-Barziv SM, Dipchand AI, Lee KJ, Cardella CJ, Benson LN, et al. ABO-Incompatible Heart Transplantation in Infants. *N Engl J Med.* 2001;344(11):793-800.
5. Chang AT, Platt JL. The role of antibodies in transplantation. *Transplant Rev.* 2009;23(4):191-8.
6. Kahwaji J, Vo AA, Jordan SC. ABO blood group incompatibility: a diminishing barrier to successful kidney transplantation? *Expert Review of Clinical Immunology.* 2010;6(6):893(8).
7. Cooper DKC. Clinical survey of heart transplantation between ABO blood group-incompatible recipients and donors. *J Heart Transplant.* 1990;9:376-81.
8. Almond C, Thiagarajan RR, Piercey GE, Gauvreau K, Blume ED, Bastardi H, et al. Waiting List Mortality Among Children Listed for Heart Transplantation in the United States. *Circulation.* 2009;119:717-27.
9. West LJ. Defining critical windows in the development of the human immune system. *Hum Exp Toxicol.* 2002;21(9-10):499-505.
10. Fan X, Ang A, Pollock-Barziv SM, Dipchand AI, Ruiz P, Wilson G, et al. Donor-specific B-cell tolerance after ABO-incompatible infant heart transplantation. *Nat Med.* 2004;10(11):1227-33.
11. Owen RD. Immunogenetic Consequences of Vascular Anastomoses between Bovine Twins. *Science.* 1945;102(2651):400-1.

12. Burnet FM, Fenner F. *The Production of Antibodies*. Melbourne, Australia: Macmillan and Co., Ltd.; 1949.
13. Billingham RE, Brent L, Medawar PB. Actively Acquired Tolerance of Foreign Cells. *Nature*. 1953;172(4379):603-6.
14. West LJ. B-cell Tolerance following ABO-Incompatible Infant Heart Transplantation. *Transplantation*. 2006;81(3):301-7 10.1097/01.tp.0000203829.78700.f3.
15. Rio-Echevarria IM, Selvestrel F, Segat D, Guarino G, Tavano R, Causin V, et al. Highly PEGylated silica nanoparticles: "ready to use" stealth functional nanocarriers. *J Mater Chem*. 2010;20(14):2780-7.
16. Radu A, Eleonora C, Lucian A, Georgeta C, Virginia V, Cristiana T. In vitro biocompatibility testing of implantable biomaterials. *Rom Biotech Lett*. 2008;13(4):3863-72.
17. Ow H, Larson DR, Srivastava M, Baird BA, Webb WW, Wiesner U. Bright and Stable Core-Shell Fluorescent Silica Nanoparticles. *Nano Lett*. 2004;5(1):113-7.
18. Almeida JPM, Chen AL, Foster A, Drezek R. In vivo biodistribution of nanoparticles. *Nanomedicine*. 2011;6(5):815-35.
19. Jabir NR, Tabrez S, Ashraf GM, Shakil S, Damanhour GA, Kamal MA. Nanotechnology-based approaches in anticancer research. *Int J Nanomed*. 2012;7:4391-408.
20. Schlatter P, K<sup>n</sup>ig MF, Karlsson LM, Burri PH. Quantitative Study of Intussusceptive Capillary Growth in the Chorioallantoic Membrane (CAM) of the Chicken Embryo. *Microvasc Res*. 1997;54(1):65-73.
21. Chen HM, Wang CS, Li MJ, Sanchez E, Li J, Berenson A, et al. A novel angiogenesis model for screening anti-angiogenic compounds: The chorioallantoic membrane/feather bud assay. *Int J Oncol*. 2010;37(1):71-9.
22. Li YJ, Duan CL, Liu JX, Xu YG. Pro-angiogenic actions of Salvianolic acids on in vitro cultured endothelial progenitor cells and chick embryo chorioallantoic membrane model. *J Ethnopharmacol*. 2010;131(3):562-6.
23. Yurlova EI, Rubina KA, Sysoeva VY, Sharonov GV, Semina EV, Parfenova EV, et al. T-cadherin suppresses the cell proliferation of mouse melanoma B16F10 and tumor angiogenesis in the model of the chorioallantoic membrane. *Russ J Dev Biol*. 2010;41(4):217-26.
24. Cimpean AM, Ribatti D, Raica M. The chick embryo chorioallantoic membrane as a model to study tumor metastasis. *Angiogenesis*. 2008;11(4):311-9.
25. Cimpean AM, Ribatti D, Raica M. THE CHICK EMBRYO CHORIOALLANTOIC MEMBRANE AS AN IN VIVO MODEL FOR STUDY TUMOR ANGIOGENESIS AND METASTASIS. *Anticancer Res*. 2008;28(5C):118.
26. Richardson M, Liu LY, Dunphy L, Wong D, Sun YM, Viswanathan K, et al. Viral serpin, Serp-1, inhibits endogenous angiogenesis in the chicken chorioallantoic membrane model. *Cardiovascular Pathology*. 2007;16(4):191-202.
27. Tufan AC, Lale Satiroglu-Tufan N. The Chick Embryo Chorioallantoic Membrane as a Model System for the Study of Tumor Angiogenesis, Invasion and Development of Anti-Angiogenic Agents. *Curr Cancer Drug Targets*. 2005;5(4):249-66.
28. Willey CD, Burleson TM, Zhai L, Anderson JC. The Development of a Chorioallantoic Membrane-tumor Xenograft Model for Tumor Vascular Targeting with Radiation. *International Journal of Radiation Oncology Biology Physics*. 2010;78(3):S624-S5.
29. Tan Q, Steiner R, Hilbe M, Hillinger S, Weder W, Lu S. Tissue engineered tumor cultured on chick embryo chorioallantoic membrane (CAM): a new model of spontaneous metastasis. *Journal of Thoracic Oncology*. 2009;4(9):S639-S40.

30. Deryugina EI, Quigley JP. Chick embryo chorioallantoic membrane model systems to study and visualize human tumor cell metastasis. *Histochem Cell Biol.* 2008;130(6):1119-30.
31. Gabrielli MG, Accili D. The Chick Chorioallantoic Membrane: A Model of Molecular, Structural, and Functional Adaptation to Transepithelial Ion Transport and Barrier Function during Embryonic Development. *J Biomed Biotechnol.* 2010.
32. Slodownik D, Grinberg I, Spira RM, Skornik Y, Goldstein RS. The human skin/chick chorioallantoic membrane model accurately predicts the potency of cosmetic allergens. *Exp Dermatol.* 2009;18(4):409-13.
33. Martinez-Madrid B, Donnez J, Van Eyck AS, Veiga-Lopez A, Dolmans MM, Van Langendonck A. Chick embryo chorioallantoic membrane (CAM) model: a useful tool to study short-term transplantation of cryopreserved human ovarian tissue. *Fertil Steril.* 2009;91(1):285-92.
34. Nap A, Groothuis PG, Punyadeera C, Hitpass LK, Kamps R, Delvoux B, et al. Contraceptives prevent the development of endometriosis in the chicken chorioallantoic membrane model. *Hum Reprod.* 2007;22:O117.
35. Nap AW, Groothuis PG, Punyadeera C, Klein-Hitpass L, Kamps R, Delvoux B, et al. Oral contraceptives prevent the development of endometriosis in the chicken chorioallantoic membrane model. *Contraception.* 2008;78(3):257-65.
36. Larger E, Marre M, Corvol P, Gasc JM. Hyperglycemia-induced defects in angiogenesis in the chicken chorioallantoic membrane model. *Diabetes.* 2004;53(3):752-61.
37. Chin WWL, Heng PWS, Lim PL, Lau WKO, Olivo M. Membrane transport enhancement of chlorin e6-polyvinylpyrrolidone and its photodynamic efficacy on the chick chorioallantoic model. *J Biophotonics.* 2008;1(5):395-407.
38. Clancy AA, Gregoriou Y, Yaehne K, Cramb DT. Measuring properties of nanoparticles in embryonic blood vessels: Towards a physicochemical basis for nanotoxicity. *Chem Phys Lett.* 2010;488(4-6):99-111.
39. Yaehne K, Tekrony, A., Clancy, A., Gregoriou, Y., Walker, J.T., Dean, K., Nguyen, T., Doiron, A., Rinker, K., Jiang, S., Childs, S., and Cramb, D. Nanoparticle Accumulation in Angiogenic Tissues: Towards Predictable Pharmacokinetics. Accepted, *Small.* 2013.
40. Diaspro A, Chirico G, Collini M. Two-photon fluorescence excitation and related techniques in biological microscopy. *Q Rev Biophys.* 2005;38(02):97-166.
41. Stober W, Fink A, Bohn E. Controlled growth of monodisperse silica spheres in the micron size range. *J Colloid Interface Sci.* 1968;26(1):62-9.
42. Larson DR, Ow H, Vishwasrao HD, Heikal AA, Wiesner U, Webb WW. Silica Nanoparticle Architecture Determines Radiative Properties of Encapsulated Fluorophores. *Chem Mater.* 2008;20(8):2677-84.
43. Schwille P, Haustein, E. Fluorescence Correlation Spectroscopy, An Introduction to its Concepts and Applications. In: Schwille P, editor. *Single Molecule Techniques: Biophysical Society*; 2002.
44. Samkoe KS, Cramb DT. Application of an ex ovo chicken chorioallantoic membrane model for two-photon excitation photodynamic therapy of age-related macular degeneration. *J Biomed Opt.* 2003;8(3):410-7.
45. Eberbeck D, et al. Aggregation behaviour of magnetic nanoparticle suspensions investigated by magnetorelaxometry. *J Phys: Condens Matter.* 2006;18(38):S2829.
46. Yaehne K, Tekrony A, Clancy A, Gregoriou Y, Walker J, Dean K, et al. Nanoparticle accumulation in angiogenic tissues: towards predictable pharmacokinetics. *Small.* 2013;9(18):3118-27.

47. Maldiney T, Richard C, Seguin J, Wattier N, Bessodes M, Scherman D. Effect of Core Diameter, Surface Coating, and PEG Chain Length on the Biodistribution of Persistent Luminescence Nanoparticles in Mice. *ACS Nano*. 2011;5(2):854-62.
48. Arnida, Jan-t-Amsbury MM, Ray A, Peterson CM, Ghandehari H. Geometry and surface characteristics of gold nanoparticles influence their biodistribution and uptake by macrophages. *Eur J Pharm Biopharm*. 2011;77(3):417-23.
49. Avgoustakis K, Beletsi A, Panagi Z, Klepetsanis P, Livaniou E, Evangelatos G, et al. Effect of copolymer composition on the physicochemical characteristics, in vitro stability, and biodistribution of PLGA-mPEG nanoparticles. *Int J Pharm*. 2003;259(1-2):115-27.
50. Ishihara T, Maeda T, Sakamoto H, Takasaki N, Shigyo M, Ishida T, et al. Evasion of the Accelerated Blood Clearance Phenomenon by Coating of Nanoparticles with Various Hydrophilic Polymers. *Biomacromolecules*. 2010;11(10):2700-6.
51. Wang M, Thanou M. Targeting nanoparticles to cancer. *Pharmacol Res*. 2010;62(2):90-9.